Title
Pullout of Geogrids from Tire Derived Aggregate Having Large Particle Size

Journal
Geosynthetics International, 27(6)

ISSN
1072-6349

Authors
Ghaaowd, I
McCartney, JS

Publication Date
2020-12-01

DOI
10.1680/jgein.20.00009

Peer reviewed

PULLOUT OF GEOGRIDS FROM TIRE DERIVED AGGREGATE HAVING LARGE PARTICLE SIZE

Ismaail Ghaaowd[1] and John S. McCartney[2]

[1] *Researcher Associate IV, Louisiana Transportation Research Center, Louisiana State University, Baton Rouge, LA, 70808, USA; Tel.: +1 225 767 9194; E-mail: ighaaowd@lsu.edu*

[2] *Professor and Department Chair, Dept. of Structural Engineering, University of California San Diego, La Jolla, CA 92093-0085, USA; Tel.: +1 858 534 9630; E-mail: mccartney@ucsd.edu*

ABSTRACT: Although tire-derived aggregate (TDA) has been used as an alternative backfill in geotechnical engineering applications, the interaction between TDA having large particle sizes (e.g., TDA with a maximum particle dimension of 300 mm) and reinforcing geosynthetics has not been studied. To address this need, this paper presents results from pullout tests on uniaxial and biaxial geogrids embedded in Type B TDA using a new large-scale pullout device having internal areal dimensions of 1220 mm in width and 3048 mm in length that can accommodate TDA layers having a height up to 1470 mm. Normal stresses ranging from 10 to 60 kPa were applied to TDA layers using dead weights atop a rigid plate and the pullout force was applied via hydraulic actuators operated in displacement-control to a bolted-epoxy sandwich-type grip mounted on slide bearings that permit pullout displacements of up to 810 mm. The maximum pullout force increased with normal stress with a displacement at maximum pullout force ranging from 100 to 350 mm. Internal displacements measured using tell-tales indicate gradual mobilization with pullout force, and the TDA layers all contracted during geogrid pullout. Uniaxial and biaxial geogrids with square-shaped apertures showed higher pullout capacity than uniaxial geogrids with rectangular-shaped apertures, but they experienced combined tensile-pullout failure at higher normal stresses.

KEYWORDS: Geosynthetics, Geogrids, Pullout, Tire derived aggregate

1. INTRODUCTION

The quantity of discarded tires has increased around the world proportional to the increase in the number of the cars. These discarded tires must be disposed of properly or reused, as they may detrimentally affect the environment. An established reuse option in civil engineering involves shredding the tires and using them as a backfill material (Humphrey 2005, 2008). In the case that they are used monolithically without being mixed with soil, these tire shreds are referred to as tire-derived aggregate (TDA). TDA is classified based on the maximum particle dimension as Type A and Type B materials (ASTM 6270). Type B TDA includes particles with a maximum dimension of up to 300 mm and requires less processing to create, making it more cost-effective than Type A TDA for earth fill applications. Larger particles also decrease the amount of exposed steel, which reduces the potential for self-heating (Humphrey 2005). The low unit weight, high thermal insulation capacity, and high permeability of TDA are distinctive properties that provide several advantages for using TDA in civil engineering applications (Humphrey 2005, 2008). Further, Ghaaowd et al. (2017) and McCartney et al. (2017) found that TDA has similar shear strength properties to granular soils and also has high damping ratio. TDA has been used widely in different civil engineering applications including subgrade replacement and backfills for embankments, retaining walls and trenches (Ahmed and Lovell 1993; Bosscher et al. 1993; Bosscher et al. 1997; Tweedie et al. 1998; Yoon et al. 2006; Humphrey 2008; Geisler et al. 1989; Lee et al. 1999; Tandon et al. 2009; Meles et al. 2013; Ahn and Cheng 2014; CalRecycle 2015; Mahgoub and El Naggar 2019). These studies have found the performance of TDA backfill to be comparable to or better than granular soil backfill. Due to its high damping ratio, TDA has also been used in seismic protection systems for foundations or waterfront structures (Hazarika et al. 2008; Tsang 2008; Senetakis et al. 2009).

When TDA is used in embankments and retaining walls, it may be used in tandem with geosynthetic reinforcements to form mechanically-stabilized TDA (MS-TDA) walls (Xiao et al. 2012). The pullout interaction between geogrids and tire chips as well as soil-tire chip mixtures is an important topic related to MS-TDA walls that has been studied by several researchers (Bernal et al. 1996, 1997; Tatlisoz et al. 1998; Tanchaisawat et al. 2010). Other studies have also evaluated the interaction between geosynthetics and tire mats (O'Shaughnessy and Garga 2000) and the interaction between metallic reinforcements and tire shreds (Youwai et al. 2004). In general, the studies focusing on tire chips found the maximum pullout force increases with increasing normal stress and found that geogrid-tire chip interaction is generally similar to geogrid-soil interaction. It should be noted however that the tire chips investigated in these studies are smaller than both Type A and Type B TDA. A general conclusion from all of the pullout studies is that larger displacements may need to be applied than when measuring the pullout resistance of geogrids in different forms of waste tires compared to geogrids in soil. The need for applying large displacements is consistent with an evaluation of direct shear tests on Type B TDA by Ghaaowd et al. (2017), who found that displacements on the order of 400 mm may be needed to mobilize the peak shear strength of Type B TDA. Fox et al. (2018) also found that large-scale containers are required to investigate the pullout response of geogrids from Type B TDA due to the large particle sizes of this material. Xiao et al. (2013) performed direct shear tests on the interface between Type A TDA and a high-density polyurethane (HDPE) uniaxial geogrid and found that the interface friction angle was 18.8°, approximately 17° smaller than the internal friction angle of Type A TDA. This emphasizes the importance of understanding the potential for TDA-geogrid interaction using pullout testsd.

This paper presents the results from pullout tests on different uniaxial and biaxial geogrids embedded in Type B TDA performed in a new large-scale pullout device. The objectives of performing these tests are to understand the impact of aperture shape on the pullout response of geogrids from Type B TDA, and to understand the necessary displacements necessary to mobilize the pullout resistance of geogrids in Type B TDA. Although uniaxial geogrids are primarily used in MS-TDA walls, the locations around corners and near the surface may be reinforced with biaxial geogrids. In addition to uniaxial and biaxial geogrids having very different tensile strengths, the pullout response of different types of geogrids (uniaxial, biaxial) having different aperture sizes in TDA is not well understood. This device was built upon the direct shear/simple shear device developed by Fox et al. (2018) and used by Ghaaowd et al. (2017) to study the internal and interface shear strength of Type B TDA and by McCartney et al. (2017) to study the cyclic shearing properties of Type B TDA.

2. BACKGROUND

Geosynthetic pullout testing is used for two purposes: (i) to evaluate the interaction between a backfill material and a geosynthetic reinforcement, and (ii) to measure the pullout strength of a geosynthetic reinforcement for application in the design of MS-TDA walls. In MSE walls, the internal stability is typically considered by assuming formation of an active Rankine failure wedge in the reinforced backfill (Christopher et al. 1990). This failure wedge is assumed to intersect the toe of the wall and extend at an angle from horizontal of $(45°+\phi/2)$ upward into the backfill, where ϕ is the friction angle of the backfill. In the upper portions of the wall, geosynthetic reinforcements should extend beyond the active Rankine failure wedge by a sufficient anchorage distance to avoid pullout failure. A general rule-of-thumb in the design of MSE walls is that the length of reinforcements should be 0.7 times the height H of the wall, but pullout testing is needed to confirm this rule-of-thumb for different geogrids in MS-TDA walls.

As in direct shear tests, the normal stress is expected to have a significant effect on the pullout response of reinforcing geosynthetics. However, it is important to note that pullout of reinforcing geosynthetics is only expected in the upper portion of a MS-TDA wall. In the lower portion of the wall, pullout is not expected due to the longer anchorage distance behind the active Rankine failure wedge. Instead, tensile failure of the geogrid is expected to be the dominant mode of failure in the lower part of the wall (Christopher et al. 1990). For this reason, the normal stresses in pullout tests are usually relatively small, and in this study range between 10 and 60 kPa.

Several studies have used pullout testing to evaluate soil-geogrid interaction, which were useful to understand the testing details that could affect the results from pullout tests (Ingold et al. 1983; Palmeira and Milligan 1989; Farrag et al. 1993; Palmeira 2004). These studies identified details on the minimum size of a pullout box with respect to the geometry of a geogrid and provide guidance on the minimum distances from the geogrid to the sides of the box. A sleeve is also required near the front face of the pullout box to minimize passive bearing pressure. The pullout geometry restrictions are summarized in ASTM D6706. Although these geometric constraints were developed for soil, they are assumed to be valid for Type B TDA as it behaves in a similar manner to granular soils. In most pullout box configurations, a rectangular box is used with a slit in one of the vertical sides with shorter dimension. The box is filled with backfill material to mid-height, the geogrid is placed atop the backfill material so that one end extends out of the slit in the side of the box, and the box is filled with backfill material. Normal stresses are applied using a pressurized air bladder or a rigid plate. A sandwich clamp grip or roller grip is used to grip the geogrid to apply pullout loads. Tell-tales extending from the back of the box may be attached to different points along the geogrid to measure the distribution of displacement along the length of the geogrid during pullout, as the geogrid may stretch while being pulled out.

Ingold et al. (1983) tested Netlon 1168 and FBM5 geogrids embedded in sand within a pullout box with plan dimensions of 500×285 mm and a height of 300 mm. A course-to-medium Boreham Wood Pit sand with a unit weight of 18.3 kN/m^3 was used. Ingold et al. (1983) defined the geogrid interface shear strength as the maximum pullout force divided by twice the embedded geogrid plane area (i.e., the top and bottom of the geogrid). The geogrid interface shear strength versus normal stress curves from this study are nonlinear for both geogrids at normal stresses less than 30 kPa, with one of the geogrids reaching a limiting pullout value while the other increasing linearly after this normal stress. The friction angle of the backfill soil is shown in the figures for comparison. Farrag et al. (1993) used a pullout box with inner dimensions of 1520 mm long, 900 mm wide, and 760mm high to test Tensar SR2 and Conwed 9027 geogrids embedded in poorly graded sand having maximum and minimum unit weights of 17.4 and 15.6 kN/m^3, respectively. For both geogrid types, the peak value of the pullout load versus displacement curves increased with increasing normal stress.

Geogrid interactions with tire chips and soil-tire chip mixtures were studied by Tatlisoz et al. (1998) using a steel pullout box having dimensions of 1520 mm long, 610 mm wide, and 16 410 mm high. Five backfill materials were used: pure tire chips, sand-30% tire chips, sandy silt-30% tire chips, sand, and silty sand. The tire chips had particle sizes ranging from 30 to 110 mm and a specific gravity of 1.2. The backfills were compacted to a dry unit weight of 5.9 kN/m^3. The maximum pullout capacity of the geogrid embedded in the sand mixed with 30% tire chips was higher in comparison to the geogrid embedded in pure sand. Similar results were founded in the case of the sandy silt soil. For both cases, the behavior of the geogrid embedded in soil-tire chip mixture and behavior of the geogrid embedded in pure soil was the similar in both cases. Tatlisoz et al. (1998) applied pullout displacements up to 100 mm and defined the pullout capacity as the maximum pullout force or the pullout force observed at a displacement of 100 mm, whichever is greater. The results indicate that the maximum pullout force increases with normal stress, with a slight nonlinearity observed for some of the backfill materials. Also, the geogrid-tire chip interaction was observed to be similar to the geogrid-soil interaction.

Lopes and Ladeira (1997) investigated the impact of backfill unit weight on the pullout results, using well-graded, gravely sand in their tests having maximum and minimum unit weights of 18.9 and 16.1 kN/m^3 receptively, and a Tensar SR55 geogrid specimen with dimensions of 330 mm width and 960 mm embedded length was tested. Two tests were performed with backfill soil having unit weights of 17.5 and 18.5 kN/m^3. The pullout force versus displacement curves from both tests are shown in Figure 2.4(a). The results indicate that the pullout force increases with increasing backfill unit weight. The impact of unit weight was also investigated by Farrag et al. (1993) for pullout of a Tensar SR2 geogrid from sand. Consistent with the observations of Lopes and Ladeira (1997), the peak of the pullout force versus displacement curves increased with increasing unit weight.

The influence of testing speed on the pullout test response of a Tensar SR2 geogrid embedded in sand was investigated by Farrag et al. (1991). The results showed the peak pullout load versus displacement rate for displacement rates ranging from 2 to 20 mm/min. The peak pullout load was found to decrease with increasing displacement rate for this geogrid and soil. However, Lopes and Ladeira (1997) performed similar tests and observed the opposite trend. Four pullouts tests performed under displacement rates ranging from 1.8 to 22 mm/min led to peak pullout loads ranging from 28.9 to 38 kN/m, respectively. Generally, the shear strength of soils will increase with increasing displacement rate.

The impact of the width of the geogrid specimen on the pullout response was evaluated by

Ochiaia et al. (1996) using a pullout box with plan dimensions of 600 × 400 mm and a height of 400 mm. A sand having a relative density of 80% and maximum and minimum void ratios of 0.97 and 0.60, respectively was used in the tests. Three tests were done on uniaxial polymer geogrid specimens with different widths. The influence of the side resistance on the pullout load of geogrid was significant when specimen width was same as the pullout box width (B/B_0 =1, where B is the specimen width, and B_0 is the pullout box width). Similar results were observed by Farrag et al. (1993), who tested four Tensar SR2 geogrids with different widths of 300, 450, 600, 750 mm embedded in sand tested in the same pullout box described above. An obvious reduction in the pullout load was observed when the specimen width increased to 750 mm, because the specimen had only 150 mm clearance on each side between the edge of the specimen and the pullout box side wall. These results indicate that the proximity of the geogrid to the side wall led to the mobilization of friction on the side walls that affected the capacity. In case that side wall friction isn't minimized using a double plastic sheet or lubricant, ASTM D6706 requires a clearance of at least 300 mm between the edge of the geogrid specimen and the side of the container.

3. MATERIALS

3.1. Tire derived aggregate

Due to the relatively flat and large size of the TDA pieces, the particle size distribution curve was defined using manual sorting of pieces having different maximum length ranges. The particle size distribution for Type B TDA is presented in Figure 1 along with characteristic particle sizes. The shape and range of particle dimesions are similar to that reported in previous studies on Type B TDA, although a few larger particles with lengths up to 320 mm in one dimension were encountered in the batch of Type B TDA used in this study. Using the characteristic particle sizes in Figure 1, the coefficient of curvature is 1.02 and the coefficient of uniformity is 2.21. The specific gravity is a particularly important parameter for TDA, as it is needed to convert the dry unit weight of TDA to commonly used geotechnical parameters like void ratio. The measured specific gravity of crumb rubber is 1.15, and submersion tests on Type B TDA give a similar value despite the presence of the wires in TDA. An advantage of TDA is that it has a lower specific gravity than soils (approximately 2.65) but is greater than that of water (1.0) so it does not float when submerged. After compaction, the dry unit weight of the Type B TDA is typically 5.64 to 8.04 kN/m^3 (Ghaaowd et al. 2017; McCartney et al. 2017), less than one-half that of most backfill soils. Ghaaowd et al. (2017) presented the shear strength parameters of Type B TDA.

3.2. Geogrids

Pullout tests were performed on two uniaxial geogrids (Tensar UX1100, referred to as GGA and Miragrid 5XT, referred to as GGB) and one biaxial geogrid (Tensar BX1500, referred to as GGC). Before the geogrids were used in the pullout tests, single-rib tensile tests were performed on samples collected from a roll and were tested following ASTM using a rate of 10 mm/min. The average values of the ultimate tensile strength along with the aperture dimensions for the different geogrids are summarized in Table 1. The geogrid specimens used in the pullout tests all had a width of 610 mm and an embedded length of 1245 mm. The geogrid specimens had an exposed length of 790 mm between the face of the Type B TDA layer and the clamps.

4. EXPERIMENTAL PROGRAM

4.1. Experimental Setup

The experimental device used in this study was originally designed by Fox et al. (2018) to permit the testing of Type B TDA in simple shear, internal direct shear, and interface direct shear modes. In this study, the device was modified to perform pullout tests to determine TDA-geogrid interaction properties. In pullout mode, the top and bottom box sections are combined into a single container using a 6x6 L beam and a C channel from the back and the front sides, respectively. Two 5X5 HSS beams were added between the two sections to create a pullout window and to support the top and bottom sleeve plates. These sleeve plates were added to reduce the passive bearing effect on the front wall on the pullout measurements, with both plates were extending the full width of the pullout box and 760 mm into the pullout box. The sleeves were at an elevation so that approximately the same TDA height would be under and above the geogrid. A bolted-epoxy sandwich clamp was developed to transfer the pullout force from the actuators to the geogrid specimen. The grip was mounted to two bearings on sliding rods to keep the actuators at same position during pullout testing. The length of the sliding rods was selected to permit pullout displacements of up to 810 mm. The main components of the device are shown in Figure 2(a), and an elevation-view cross section of the test setup is shown in Figure 2(b).

4.2. Procedures

The Type B TDA was stored in large pre-weighed bags having an average weight of 3 kN, as shown in Figure 3(a). Knowing the weight of each bag facilitated the compaction process and permitted careful control of the TDA unit weight in the large shear box. Before placement of the TDA into the box, the sides of the box were lined with 2 layers of plastic sheeting to reduce side friction effects. The Type B TDA was compacted in 100 mm-thick lifts using a rolling vibrating compactor having a weight of 14.4 kN and 6 passes per lift as shown in Figure 3(b). A temporary protective plywood was placed against the side of the compactor to avoid damaging the plastic sheeting during compaction. The Type B TDA was observed to visibly densify after compaction, indicating that it locked into a tighter structure.

After the Type B TDA was placed and compacted to the level of the bottom sleeve plate, the bottom sleeve plate and the two 5X5 HSS beams were placed respectively. More TDA was added and compacted to reach the geogrid level. The geogrid was located at an elevation of 737 mm from the box base, which was slightly above the pullout gap so that the geogrid would be centered at the pullout height after compaction of the overlying TDA lifts. Then, the geogrid specimen was connected to the clamps and laid over the TDA. Five 762 mm-long string potentiometers were connected to the geogrid at different locations shown in Figure 4(a) to act as tell-tales and measure the displacement distribution along the geogrid specimen during pullout. Aluminum protection tubes were used to protect the tell-tales during testing. Also, two 635 mm-long string potentiometers were used to measure the differential displacement of the geogrid between the TDA face at the back of the sleeves and the location of the clamp as shown in Figure 4(b). The back of the box showing the tensioned string potentiometers is shown in Figure 4(b).

The top sleeve plate and top section of the box were then placed atop the bottom section of the box. The same procedures were used to place the TDA into the top section of the box. The TDA was added until the height above the geogrid reached 737 mm. The TDA unit weight after compaction was 6.4 kN/m^3. Next, the normal stress was applied to the top of the TDA specimen using dead weights as shown in Figure 5(a). The specimen thickness was then measured after application of the normal stress. The normal stress was left on the specimen for a minimum of 12 hours (overnight) before moving to the next stage of testing. This permits any creep deformations such as those observed by Wartman et al. (2007) to be accommodated. The changes in TDA unit weight was were inferred from the vertical settlement after application of the vertical stress.

To start the pullout test, the height of the actuators was aligned with the level of the geogrid. The actuators were extended and attached to the clamps to pull the geogrid specimen toward the concrete restraining block. The instrumentation was then prepared for testing. This includes three 1270 mm external string potentiometers stretching from the reaction block to the connection beam between the actuators and the clamps to measure the horizontal displacement of the geogrid at the clamps end and to double-check the recorded actuator displacement. The other string potentiometers for the tell-tales were also connected and pre-tensioned. Four vertical displacement transducers were attached at the box corners to measure changes in TDA height during pullout. The pullout test was then started at a constant pullout displacement rate of 10 mm/min. The test was continued until the sliding bearings reached the end of the sliding track as shown in Figure 5(b). Then the actuators were extended again to their initial position. Tests were also performed to measure the error in the pullout force due to friction between the bearings and the sliding rods.

5. RESULTS

5.1. Overview

A total of 12 pullout tests were performed in this study on the three geogrids, with normal stresses ranging from approximately 10 to 60 kPa. The details of the different tests are presented in Table 2. After compaction, the specimens were loaded to different normal stresses and experienced a change in volume and total unit weight. The relationship of the TDA unit weight after application of the normal stress (i.e., at the beginning of shearing) is shown in Figure 6(a). A linear increase in unit weight with increasing normal stress is observed. It should be noted that because the TDA is dry, the total and dry unit weights are the same. As the specimens were loaded from the same initial void ratio, the relationship between the void ratio estimated from the dry unit weight and the applied normal stresses to the different specimens can be assumed to represent the compression curve for TDA, shown in Figure 6(b). An approximately log-linear compression curve is observed, and the calculated compression index C_c is 0.34.

5.2. Pullout Tests on GGA

A total of four tests were performed to characterize the role of the initial normal stress on the pullout resistance of the uniaxial GGA geogrid embedded in Type B TDA for normal stresses ranging from 10.1 to 58 kPa. Time series of the pullout force and tell-tale displacements are shown in Figure 7. The tell-tale locations noted within the legend are positive within the TDA and negative for the displacement sensor on the exposed geogrid outside of the TDA. In all four tests, a gradual mobilization of displacements along the length of the geogrid is observed, with a longer delay in mobilization for tell-tales further from the TDA face with increasing normal stress. The difference in displacements of the exposed geogrid at locations of 0 and -673 mm from the TDA face indicate that the geogrid stretched during pullout, with more stretching at higher normal stresses. Despite the gradual mobilization in displacements along the geogrid observed in Figure 7, GGA behaved approximately more like a rigid body for all normal stresses when compared to the other geogrids tested in this study. This is likely due to the higher stiffness of the HDPE GGA compared to the other polymers of the other geogrids. The peak pullout forces occurred at pullout displacements ranging between 200-370 mm, confirming the need for the large pullout box. A clear post-peak softening behavior is observed in all tests. The pullout force curves were not very smooth due to sudden releases in interlocking connections between the TDA particles and the geogrid apertures. This was especially the case after reaching the peak pullout force, when a sharp drop in pullout force that became more prominent with increasing normal stress.

The pullout force as a function of displacement from the four tests on GGA is shown in Figure 8(a). Sharp drops in pullout force were observed in all tests, especially after the peak pullout force was reached. These sharp drops signify interaction between the TDA particles and geogrid by friction and interlocking. Despite the relatively narrow apertures for GGA, post-test evaluations of the geogrids indicate that the TDA particles were able to enter the apertures during pullout. The volumetric strains calculated from the four vertical potentiometers on the corners of the pullout box are shown in Figure 8(b). An increase in volumetric contraction is observed with increasing normal stress, although the volumetric strains are not as significant as those observed in the direct shear tests on TDA reported by Ghaoowd et al. (2017). In the direct shear tests reported by Ghaaowd et al. (2017), the TDA was observed to initially contract to a volumetric strain of up to 0.8% at a horizontal displacement, after which dilation was observed. A dilation angle of 1.2 to 3.7° was observed for the TDA. The volumetric strains were dominated by the vertical displacements at the front two corners of the pullout box, and the vertical displacements at the back two corners were negligible.

5.3. Pullout Tests on GGB

A total of five tests were performed to characterize the role of the initial normal stress on the pullout resistance of the uniaxial GGB geogrid embedded in Type B TDA for normal stresses ranging from 19.2 to 58.1 kPa. Time series of the pullout force and tell-tale displacements are shown in Figure 9. The tell-tale locations are positive within the TDA and negative for the displacement sensor on the exposed geogrid outside of the TDA. Similar to the tests on GGA, a gradual mobilization of displacements along the geogrid is observed in tests GGB-1, GGB-2, and GGB-3. In these lower normal stress tests, the GGB specimens pulled out the TDA approximately like a rigid body. However, a change in behavior is noted in tests GGB-4 and GGB-5 at higher normal stresses. In addition to showing a more distributed mobilization in displacements across the length of the exposed and embedded geogrid, a sharp post-peak drop in pullout force was observed. Post-test observations indicate that tensile failure of the geogrid occurred in isolated ribs near the face of the TDA, possibly due to stress concentrations associated with nonuniform interaction with the TDA across the width of the geogrid. Post-test evaluations also indicate that the exposed steel wire edges on the TDA particles may penetrate and cut the polyester yarns during placement and pullout, which may have contributed to the formation of stress concentrations in some ribs at the higher normal stresses. Despite the change in pullout mode at higher normal stresses, the peak pullout forces occurred at a pullout displacement of approximately 108.5-154 mm in all five tests. This was nearly half the displacement required to mobilize the peak pullout force for GGA, indicating that GGB has a stiffer pullout response from TDA than GGA. The peak pullout forces for GGB were greater than GGA, possibly due to the approximately square apertures of GGB that may have allowed greater interaction with the TDA. Similar to GGA, the pullout force curves were not smooth due to interlocking and the post-peak softening became more pronounced with increasing normal stress.

The pullout force as a function of displacement from the four tests on GGA is shown in Figure 10(a). Despite the change in failure mode for the two tests at higher normal stresses, the shapes of the pullout curves are relatively similar before peak conditions, with a clear increase in pullout stiffness with increasing normal stress. The volumetric strains calculated from the four vertical potentiometers on the corners of the pullout box are shown in Figure 10(b). An increase in volumetric contraction is observed with increasing normal stress similar to GGA, but the test at the highest normal stress showed lower contraction than the other tests. However, this test showed more vertical displacement in one corner than the other on the front face, indicating that nonuniform pullout of the geogrid may have occurred at the highest normal stress.

5.4. Pullout Test on GGC

A total of three tests were performed to characterize the role of the initial normal stress on the pullout resistance of the biaxial GGC geogrid embedded in Type B TDA for normal stresses ranging from 9.5 to 29.3 kPa. Lower normal stresses were investigated for GGC as biaxial geogrids are expected to be used in corners near the crest of MS-TDA walls. GGC also has lower tensile strength than the uniaxial geogrids, so pullout failure is expected to dominate under lower normal stresses. Time series of the pullout force and tell-tale displacements are shown in Figure 11. The tell-tale locations are positive within the TDA and negative for the displacement sensor on the exposed geogrid outside of the TDA. Similar to the tests on GGA, a gradual mobilization of displacements along the geogrid is observed in tests GGC-1 and GGC-2. In these tests, a greater mobilization of displacements are observed across the length of the exposed and embedded geogrid for these normal stresses when compared with the uniaxial geogrids, and the biaxial geogrid only behaved approximately like a rigid body at the lowest normal stress. Similar to GGB, a change in behavior is noted in test GGC-3 at a normal stress of 29.3 kPa. Although it appeared that a peak value had been reached, tensile failure of the geogrid was observed near the TDA face. This tensile failure occurred at 35 kN/m, which is slightly below the in-air tensile strength. The failure at a slightly lower force may have occurred due to stress concentrations associated with nonuniform interaction with the TDA across the width of the geogrid. The pullout force curves were smoother than the other geogrids, with a steady rate of post-peak softening for the two tests that did not experience tensile failure. Despite the lower tensile strength of the biaxial GGC compared to the two other uniaxial geogrids, GGC had similar pullout strengths to GGB. This may have been due to the similar aperture sizes for these two geogrids reflecting similar interaction with TDA.

The pullout force as a function of displacement from the four tests on GGA is shown in Figure 12(a). Despite the change in failure mode for the two tests at higher normal stresses, the shapes of the pullout curves are similar before peak conditions, with a clear increase in pullout stiffness with increasing normal stress. The volumetric strains calculated from the four vertical potentiometers on the corners of the pullout box are shown in Figure 12(b). An increase in volumetric contraction is observed with increasing normal stress similar to GGA.

6. ANALYSIS

A comparison of the maximum pullout force as a function of normal stress for the three geogrids is shown in Figure 13(a). Despite the changes in pullout failure mode noted for GGB and GGC, slightly nonlinear relationships between maximum pullout force and normal stress are noted for all three geogrids. It is also interesting to note that the maximum pullout forces for GGB and GGC are similar. Despite the difference in polymer and tensile strength of these geogrids, they have similar apertures that are approximately square. This observation may indicate that the aperture size has an important effect on the pullout of geogrids from TDA with large particle sizes.

The maximum pullout forces were used to calculate the pullout resistance factor F, which represents the interaction between a backfill material and a geogrid, using the model of Christopher et al. (1990):

$$P_r = F \,.\, \alpha \,.\, \sigma'_v \,.\, L \,.\, C \tag{1}$$

where P_r is the maximum pullout force of the geogrid per unit width from the pullout test, α is a scale effect correction factor, L is the embedded length in the TDA which is 1.245 m for all the tests performed in this study, C is the geogrid effective unit perimeter which is 2 for the geogrid (i.e., the top and bottom of the geogrid), σ'_v is the effective vertical stress at the TDA-geogrid interface which includes the applied dead load plus the vertical stress associated with the TDA atop the level of the geogrid. The value of α is assumed to be 0.8 for extensible geogrid reinforcements (Elias et al. 2001), as all of the geogrids tested in this study showed some extension during pullout. The only other unknown variable is the pullout resistance factor, which can be obtained by rearranging Equation (1) as follows:

$$F = \frac{P_r}{\alpha \,.\, \sigma'_v \,.\, L \,.\, C} \tag{2}$$

The pullout resistance factors were calculated for the three geogrids tested, and a plot of the pullout resistance factors as a function of the normal stress normalized by the atmospheric pressure is shown in Figure 13(b). The pullout resistance factors in this figure range from 0.2 to 1.15, which are within the same range reported by Tatlisoz et al. (1998) for pullout of geogrids from both tire chips and different soils.

Power law relationships were fitted to the three sets of data and are shown Figure 13(b). As GGB was not tested at the lowest normal stresses and GGC could not be used for higher normal stresses, a single relationship was not fitted to the pullout factors for these two geogrids even though they seem to follow the same trend. Nonetheless, the similar relationships for both indicate that the similar aperture sizes and shapes may have led to similar trends in their pullout resistance factors. The fact that there are ranges in the parameters of the power law relationships emphasizes the importance of geogrid-specific testing to account for different TDA-geogrid interactions. Even though TDA could be assumed to be more consistent than different backfill soils, it is expected that the interactions with a given geogrid will be unique and related to the geogrid polymer and aperture opening size. However, the data provided here provide useful preliminary information for MS-TDA wall design.

The displacement in peak for the three geogrids are shown in Figure 13(c). An interesting observation from this data is that the uniaxial HDPE GGA had the greatest displacements at peak pullout force, while the other two geogrids had similar displacements at peak. This is possibly due to the relative contributions of interface friction and interlocking to the pullout force that lead to a gradual development of the pullout force. Xiao et al. (2013) observed a relatively low interface friction angle for a uniaxial HDPE geogrid similar to GGA. Nonetheless, the relatively large displacements at peak pullout force ranging from 100 to 350 mm indicate that MS-TDA walls will be able to withstand relatively large displacements before experiencing failure.

7. CONCLUSIONS

This paper presents results from a new large-scale pullout device focused on understanding the interaction between uniaxial and biaxial geogrid reinforcements and tire-derived aggregate (TDA) with maximum particle dimensions up to 300 mm (Type B TDA). For all the conditions tested, the pullout strength of different geogrids followed not obvious nonlinear relationship with normal stress for the range of normal stresses expected near the crest of MS-TDA walls. Pullout factor relationships with normal stress were defined for biaxial and uniaxial geogrids, and a nonlinear decreasing trend with normal stress was observed. The results indicate that the aperture size and shape had the greatest impacts on the pullout response of geogrids from TDA. The biaxial geogrid was observed to have a high pullout strength despite its lower tensile strength because of interlocking with the TDA particles, likely due to their square-shaped apertures. Although the uniaxial geogrid manufactured from HDPE had the lowest pullout resistance of the geogrids tested likely due to its thin apertures and low interface friction angle, it may have the best resistance to chemical degradation or installation damage in TDA backfills. All three geogrids were observed to have large displacements at peak pullout force ranging from 100 to 350 mm, but the uniaxial HDPE geogrid showed the greatest displacements at peak pullout. The results indicate that MS-TDA walls may be able to withstand large deformations before failure.

ACKNOWLEDGMENTS

The authors thank the Powell Laboratory staff in the Department of Structural Engineering at the University of California-San Diego for assistance with the experimental program. Financial support from California Department of Resources Recycling and Recovery (CalRecycle) is gratefully acknowledged. The assistance and support of Stacey Patenaude and Bob Fujii of CalRecycle as well as Joaquin Wright and Chris Trumbull of GHD is also gratefully acknowledged. The contents of this paper reflect the views of the authors and do not necessarily reflect the views of the sponsor.

NOTATION

Basic SI units are given in parentheses.

α	Scale effect correction factor (dim.)
C	Effective unit perimeter (dim.)
C_c	Compression index (dim.)
D_{10}	Characteristic TDA particle length (mm)
D_{30}	Characteristic TDA particle length (mm)
D_{50}	Characteristic TDA particle length (mm)
D_{60}	Characteristic TDA particle length (mm)
F	Geosynthetic-specific pullout resistance factor
L	Embedded length of the geogrid in the TDA specimen (m)
P_r	Maximum pullout force of the geogrid per unit width (kN/m)
σ'_v	Effective vertical stress (kPa)

ABBREVIATIONS

TDA	Tire derived aggregate
MS-TDA	Mechanically stabilized TDA

REFERENCES

Ahmed, I. and Lovell, C.W. (1993). "Rubber soils as lightweight geomaterials." Transportation Research Record. 1422, 61-70.

Ahn, I.-S., and Cheng, L. (2014). "Tire derived aggregate for retaining wall backfill under earthquake loading." Construction and Building Materials. 57, 105-116.

ASTM. (2017). “Standard practice for use of scrap tires in civil engineering applications.” ASTM D6270, West Conshohocken, PA.

Bernal, A., Salgado, R., Swan Jr, R.H., and Lovell, C.W. (1997). ‘‘Interaction between tire shreds, rubber-sand and geosynthetics.” Geosynthetics International. 4(6), 623-643.

Bosscher, P.J., Edil, T.B., and Eldin, N. (1993). “Construction and performance of shredded waste tire test embankment.” Transportation Research Record. 1345, 44-52.

Bosscher, P.J., Edil, T.B., and Kuraoka, S. (1997). “Design of highway embankments using tire chips.” Journal of Geotechnical and Geoenvironmental Engineering. 123(4), 295-304.

CalRecycle. (2015). Tire Derived Aggregate (TDA) Usage Guide. Edition 1.0.

Elias, V., Christopher, B.R., and Berg, R. (2001). Federal Highway Administration (FHWA) SA-00-043. Mechanically Stabilized Earth Walls and Reinforced Soil Slopes, Design & Construction Guidelines. National Highway Institute. Federal Highway Administration. Washington, D.C.

Farrag, K., Acar, Y.B., and Juran, I. (1993). “Pull-out resistance of geogrid reinforcements.” Geotextiles and Geomembranes. 12(2), 133–159.

FHWA. (1990). Reinforced Soil Structures: Design and Construction Guidelines. FHWA-RD-89-043. U.S. Department of Transportation Federal Highway Administration.

FHWA. (1996). Laboratory Study on the Use of Tire Shreds and Rubber-Sand in Backfills and Reinforced Soil Applications. FHWA-IN-JHRP-96-12. U.S. Department of Transportation Federal Highway Administration.

Fox, P.J., Thielmann, S.S., Sanders, M.J., Latham, C., Ghaaowd, I., and McCartney, J. S. (2018). “Large-scale combination direct shear/simple shear device for tire-derived aggregate.” ASTM Geotechnical Testing Journal. 41(2), 340-353.

Ghaaowd, I., McCartney, J.S., Thielmann, S., Sanders, M. and Fox, P.J. (2017). "Shearing behavior of tire derived aggregate with large particle sizes. I: Internal and concrete interface direct shear behavior." J. of Geotech. and Geoenv. Eng. 143(10), 04017078.

Geisler, E., Cody, W.K., and Niemi, M.K. (1989). "Tires for subgrade support." Annual Conference on Forest Engineering, Coeur D'Alene, ID. 1-5.

Hazarika, H., Kohama, E., and Sugano, T. (2008). "Underwater shake table tests on waterfront structures protected with tire chips cushion." Journal of Geotechnical and Geoenvironmental Engineering. 134(12), 1706–1719.

Humphrey, D.N. (2005). "Tire derived aggregate - A new road building material," Proceedings, 7th International Conference on the Bearing Capacity of Roads, Railways and Airfields, Trondheim, Norway, 27-29 June, 6 pp. [CDROM]

Humphrey, D.N. (2008). "Tire derived aggregate as lightweight fill for embankments and retaining walls." Scrap Tire Derived Geomaterials—Opportunities and Challenges, H. Hazarika and K. Yasuhara, eds., Taylor & Francis Group, London.

Ingold, T.S. (1983). "Laboratory of pull-out testing of geogrid reinforcements in sand." Geotechnical Testing Journal. ASTM, 6(3), 101-11.

Lee, J.H., Salgado, R., Bernal, A., and Lovell, C.W. (1999). "Shredded tires and rubber-sand as lightweight backfill." Journal of Geotechnical and Geoenvironmental Engineering, 125(2), 132–141.

Lopes, M.L. and Ladeira, M. (1996). "Role of specimen geometry, soil height and sleeve length on the pull-out behaviour of geogrids." Geosynthetics International. 3 (6), 701–719.

Mahgoub, A., and El Naggar, H. (2019). "Using TDA as an engineered stress-reduction fill over preexisting buried pipes." Journal of Pipeline Systems Engineering and Practice. 10(1), 04018034.

McCartney, J.S., Ghaaowd, I., Fox, P.J., Sanders, M., Thielmann, S., and Sander, A. (2017). "Shearing behavior of tire derived aggregate with large particle sizes. II: Cyclic simple shear behavior." J. of Geotech. and Geoenv. Eng. 143(10), 04017079.

Meles, D., Bayat, A., Shafiee, M.H., Nassiri, S. and Gul, M. (2013). "Field study on construction of highway embankment made from two tire derived aggregate types and tire-derived aggregate mixed with soil as fill materials." In Transportation Research Board, 92 Annual Meeting. Washington, DC.

Ochiai, H., Otani, J., Hayashic, S., and Hirai, T. (1996). "The pullout resistance of geogrids reinforced soil." Geotextiles and Geomembranes, 14(1), 19-42.

O'Shaughnessy, V. and Garga, V.K. (2000). "Tire-reinforced earthfill. Part 2: Pull-out behavior and reinforced slope design." Canadian Geotechnical Journal. 37, 97-116.

Palmeira, E.M. and Milligan, G.W.E. (1989). "Scale and other factors affecting the results of pullout tests of grids buried in sand." Géotechnique. 39(3), 511-524.

Palmeira, E.M. (2004). "Bearing force mobilization in pull-out tests on geogrids.'' Geotextiles and Geomembranes. 22(6), 481–509.

Senetakis, K., Anastasiadis, A., Trevlopoulos, K, Pitilakis, K. (2009). "Dynamic response of SDOF systems on soil replaced with sand/rubber mixture." Proceedings of the ECOMAS thematic conference on computation methods in structural dynamics and earthquake engineering. 22-24.

Tanchaisawat, T., Bergado, D.T., Voottipruex, P., and Shehzad, K. (2010). “Interaction between geogrid reinforcement and tire chip–sand lightweight backfill.” Geotextiles and Geomembranes. 28, 119-127.

Tandon, V., Velazco, D. A., Nazarian, S., and Picornell, M. (2007). “Performance monitoring of embankments containing tire chips: Case study.” J. Perform. Constr. Facil., 10.1061/(ASCE)0887-3828(2007) 21:3(207), 207–214.

Tatlisoz, N., Edil, T.B., and Benson, C.H. (1998). “Interaction between reinforcing geosynthetics and soil-tire chip mixtures.” J. of Geotech. and Geoenv. Eng. 124(11), 1109-1119.

Tsang, H.H. (2008). “Seismic isolation by rubber–soil mixtures for developing countries.” Earthquake Engineering and Structural Dynamics. 37(2), 283–303.

Tweedie, J.J., Humphrey, D.N., and Sandford, T.C. (1998). “Tire shreds as light-weight retaining wall backfill, active conditions.” J. of Geotech. and Geoenv. Eng. 124(11), 1061-1070.

Xiao, M., Bowen, J., Graham, M., and Larralde, J. (2012). “Comparison of seismic responses of geosynthetically-reinforced walls with tire-derived aggregates and granular backfills.” J. Mater. Civil Eng., 10.1061 /(ASCE)MT.1943-5533.0000514, 1368–1377

Xiao, M., Ledezma, M., and Hartman, C. (2013). “Shear resistance of tire derived aggregate using large-scale direct shear tests.” J. Mater. Civil Eng., 10.1061/(ASCE)MT.1943-5533.0001007, 04014110.

Yoon, S., Prezzi, M., Siddiki, N. Z., and Kim, B. (2006). “Construction of a test embankment using a sand-tire shred mixture as fill material.” Waste Management. 26, 1033-1044.

Youwai, S., Bergado, T., and Supawiwat, N. (2004). “Interaction between hexagonal wire reinforcement and rubber tire chips with and without sand mixture.” ASTM Geotechnical Testing Journal. 27(3), 260-268.

Table 1: Geogrid property summary

Geogrid Designation	Type	Polymer	Aperture Dimensions (mm)	Maximum Tensile Load (kN/rib)	Maximum Tensile Load (kN/m)
GGA	Uniaxial	High density polyurethane	424.2 (machine direction), 17 (cross-machine direction)	1.2	53.3
GGB	Uniaxial	Polyester yarns with PVC coating	22.2 (machine direction), 25.4 (cross-machine direction)	1.9	71.6
GGC	Biaxial	Polypropylene	25 (machine direction), 30.5 (cross-machine direction)	1.2	36.8

Table 2. Pullout testing summary

Test No	Initial TDA Unit Weight (kN/m^3)	Initial TDA Void Ratio	Displacement Rate (mm/min)	Initial Normal Stress (kPa)	Max Pullout Force (kN/m)	Displacement at Peak Pullout Force (mm)
GGA-1	6.6	0.97	10	10.1	11.7	242.3
GGA-2	6.8	0.89	10	19.2	13.9	199.6
GGA-3	6.9	0.80	10	38.5	22.3	365.7
GGA-4	7.2	0.71	10	58.1	25.8	368.0
GGB-1	6.2	0.99	10	19.2	25.1	108.5
GGB-2	6.5	0.89	10	29.4	35.8	154.0
GGB-3	6.7	0.85	10	38.6	37.5	144.4
GGB-4	6.8	0.8	10	47.9	49.2	134.5
GGB-5	7.1	0.72	10	58.1	54.3	133.2
GGC-1	6.1	1.03	10	9.5	21.6	89.7
GGC-2	6.3	0.94	10	19.4	28.4	155.0
GGC-3	6.5	0.90	10	29.3	32.6	201.8

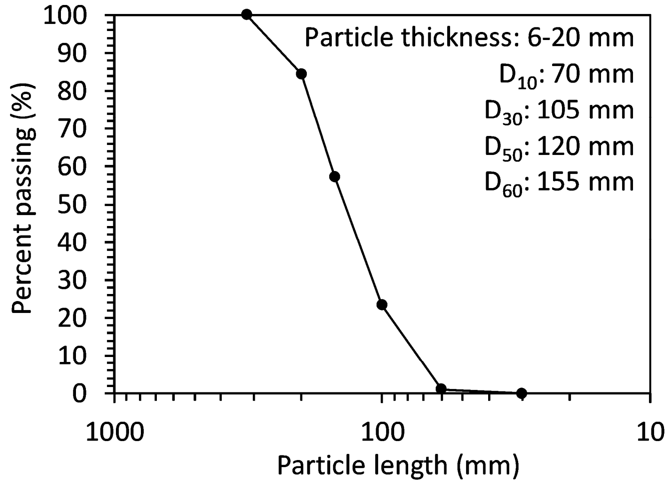

Figure 1: Particle size distribution for the Type B TDA aggregate

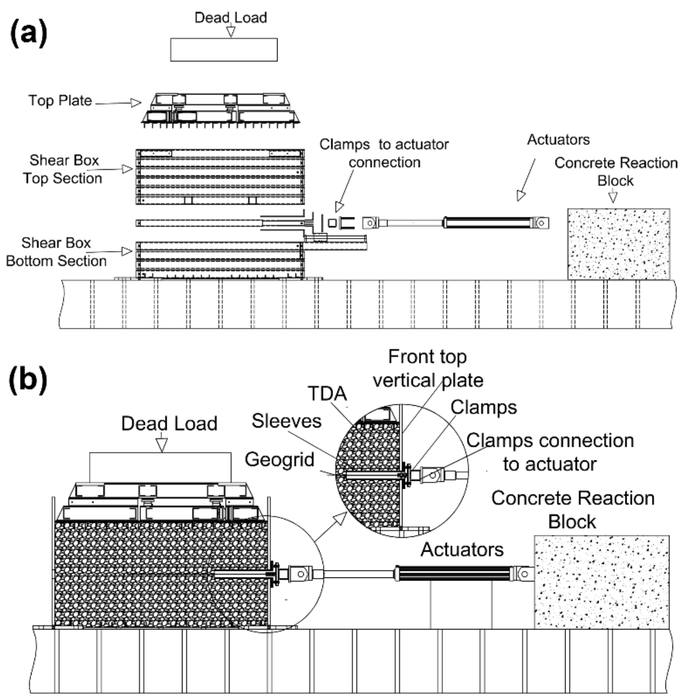

Figure 2: Pullout device schematics: (a) Components: (b) Assembled cross-section

(a)

(b)

Figure 3: TDA placement in the bottom section of the box: (a) Pre-weighed bags of TDA with lift markers; (b) leveling of TDA lists prior to compaction

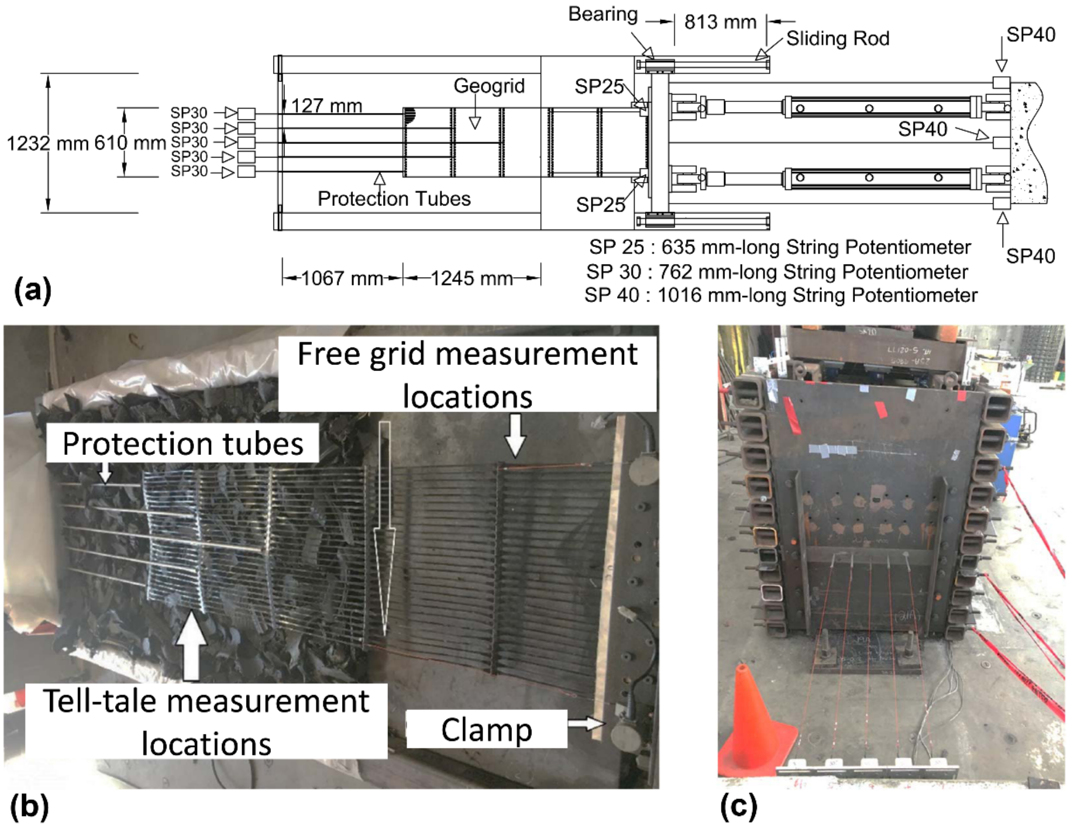

Figure 4. (a) Tell-tale locations attached to the external string potentiometers; (b) Picture of tell-tale connections, protection tubes, and geogrid clamping system; (c) Tell-tales exiting back of box connected to string potentiometers

(a)

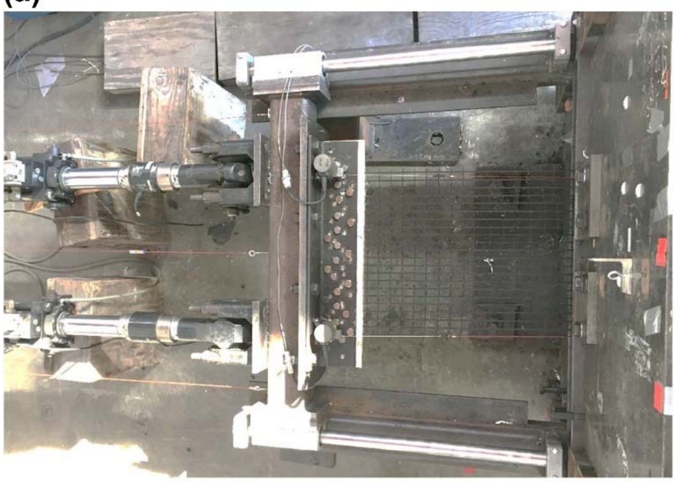

(b)

Figure 5: (a) Picture of the pullout box showing the top plate and dead load for higher normal stresses; (b) Top-down view of grip system after 735 mm of pullout displacement

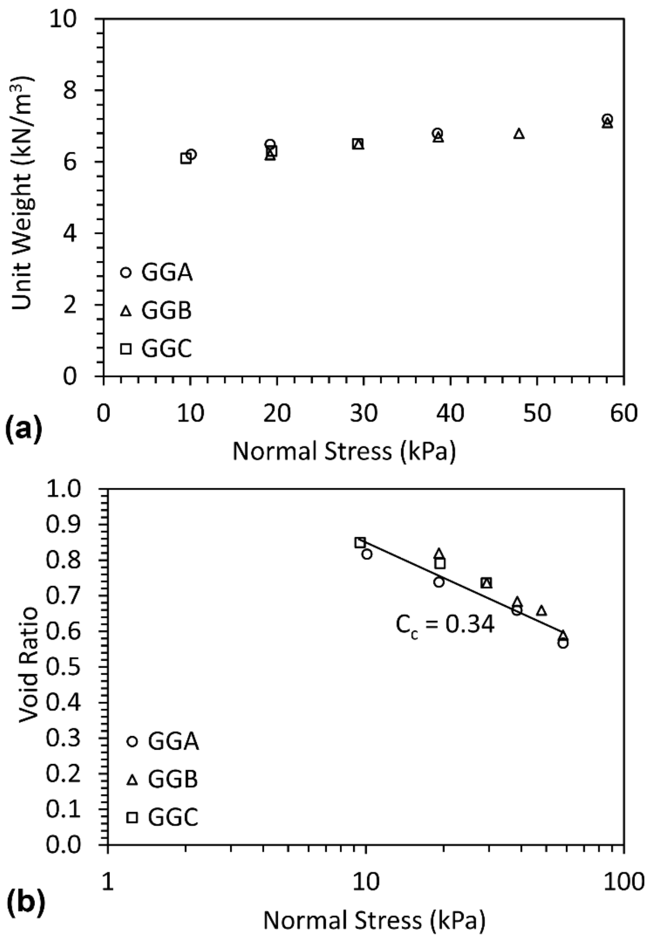

Figure 6: (a) TDA unit weights after application of the normal stress in all geogrid pullout tests; (b) Estimated TDA compression curve based on unit weight measurements

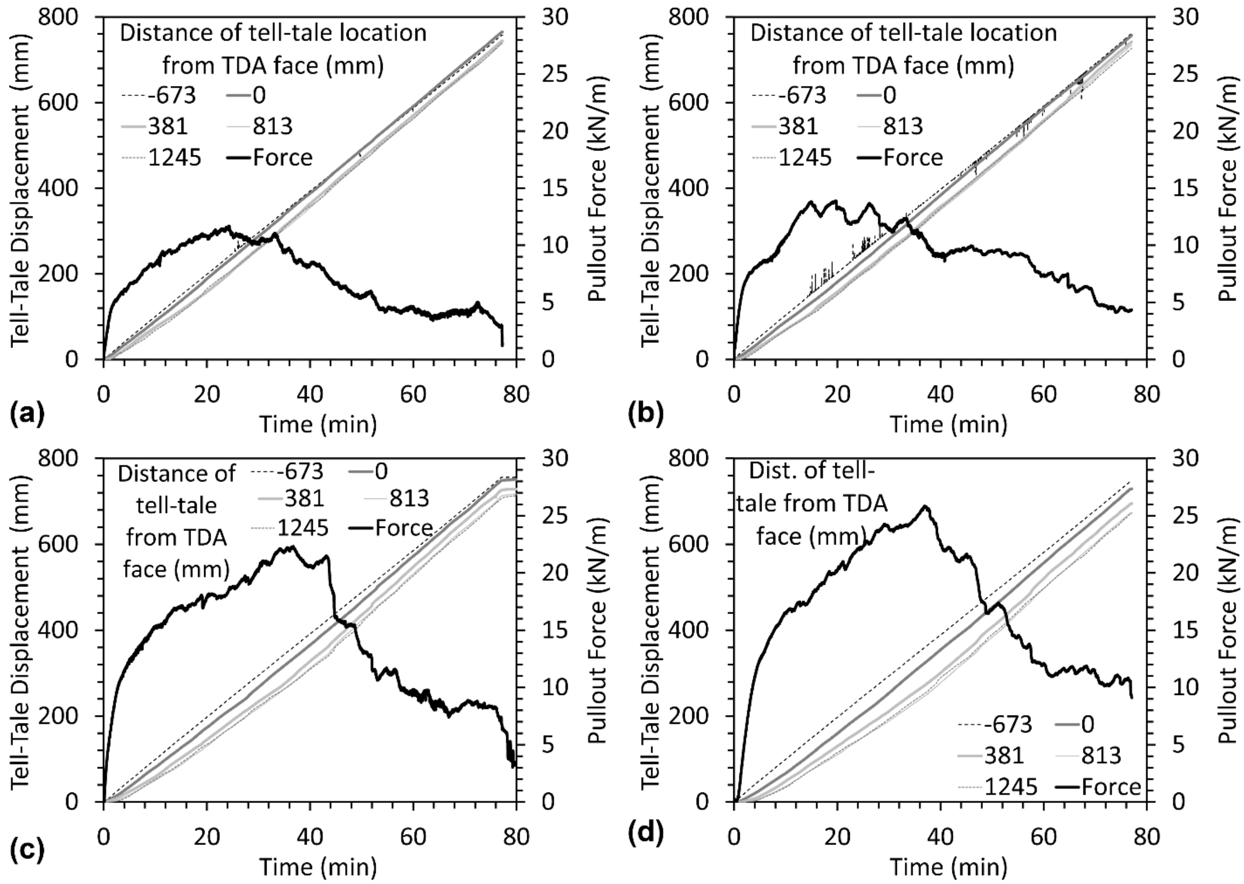

Figure 7: Pullout time series for GGA tests: (a) GGA-1; (b) GGA-2; (c) GGA-3; (d) GGA-4

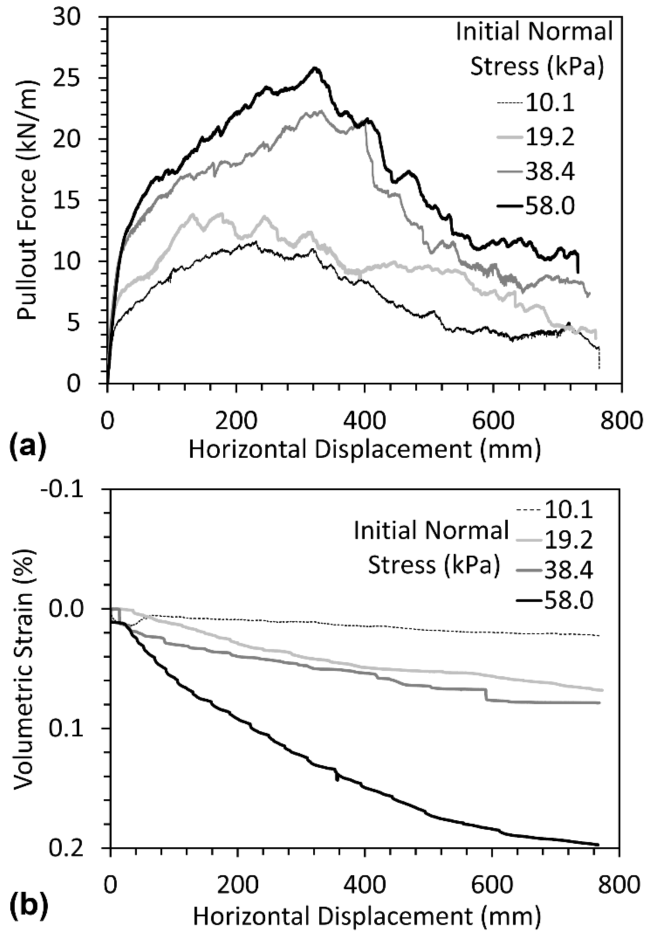

Figure 8: Pullout results for GGA: (a) Pullout force-displacement curves; (b) Volumetric strain-displacement curves

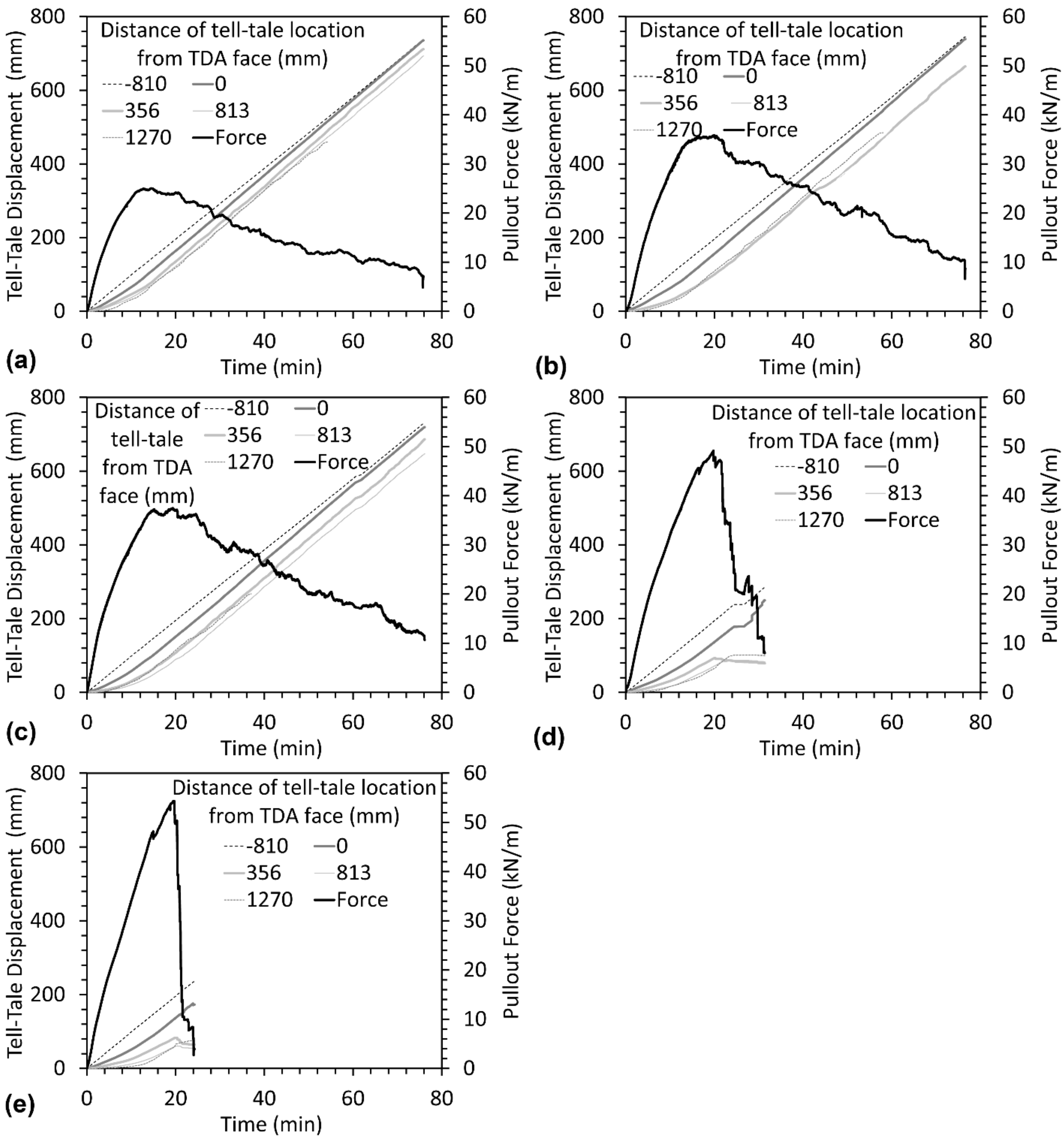

Figure 9: Pullout time series for GGB tests: (a) GGB-1; (b) GGB-2; (c) GGB-3; (d) GGA-4; (e) GGA-5

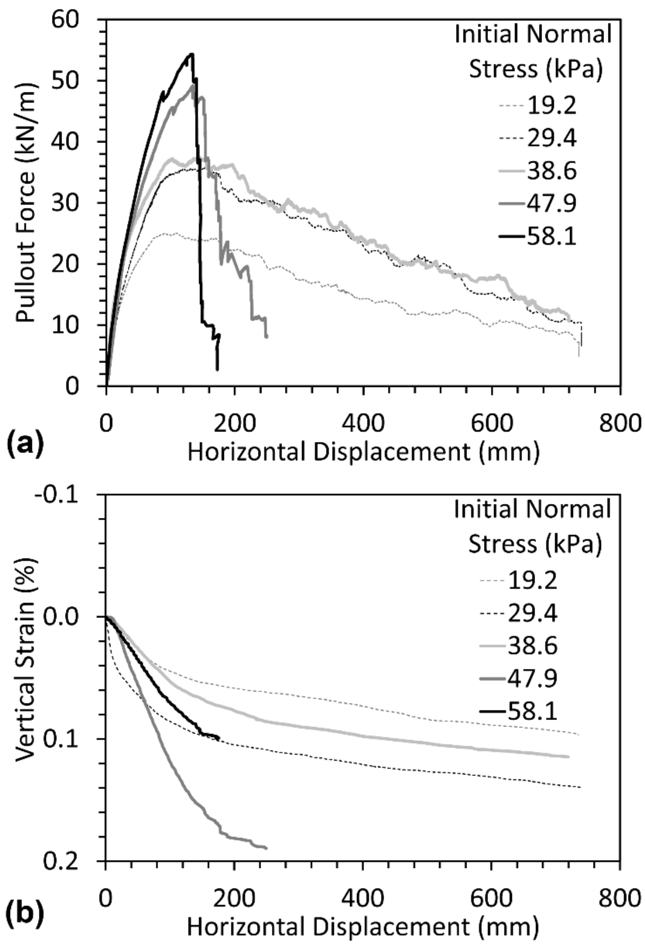

Figure 10: Pullout results for GGB: (a) Pullout force-displacement curves; (b) Volumetric strain-displacement curves

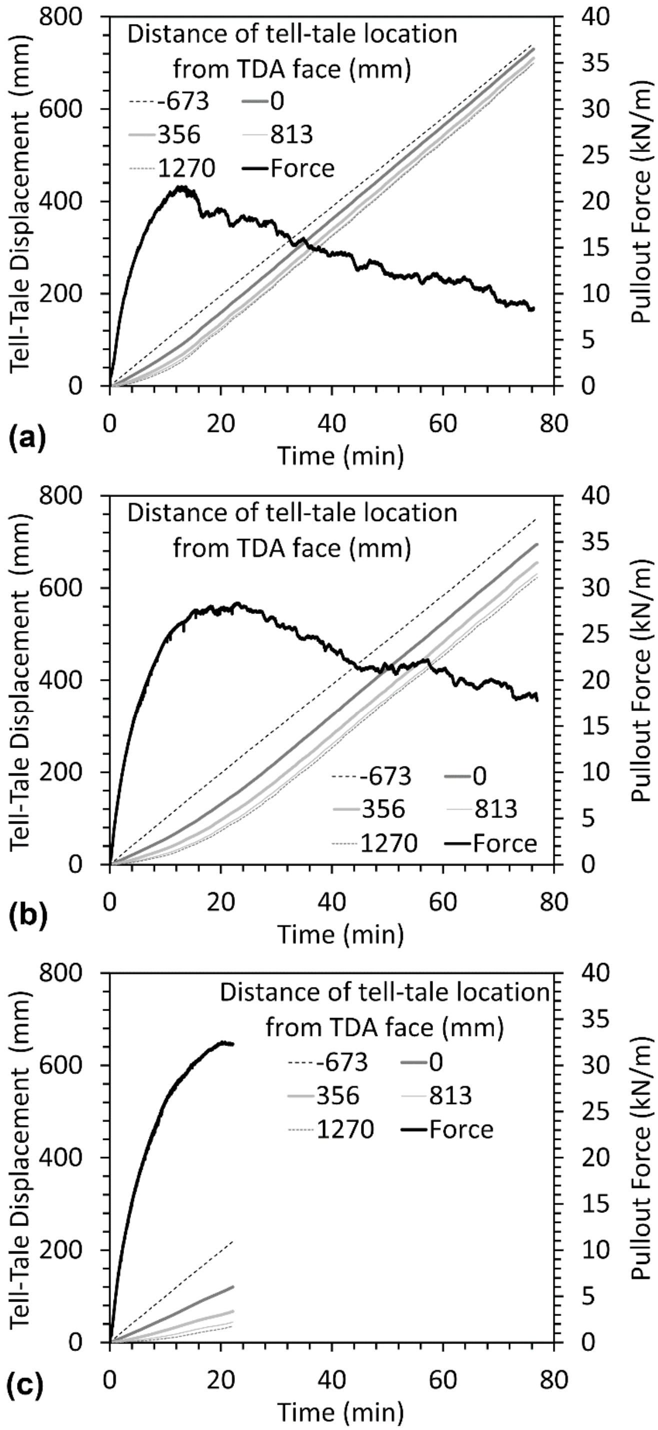

Figure 11: Pullout time series for GGC tests: (a) GGC-1; (b) GGC-2; (c) GGC-3

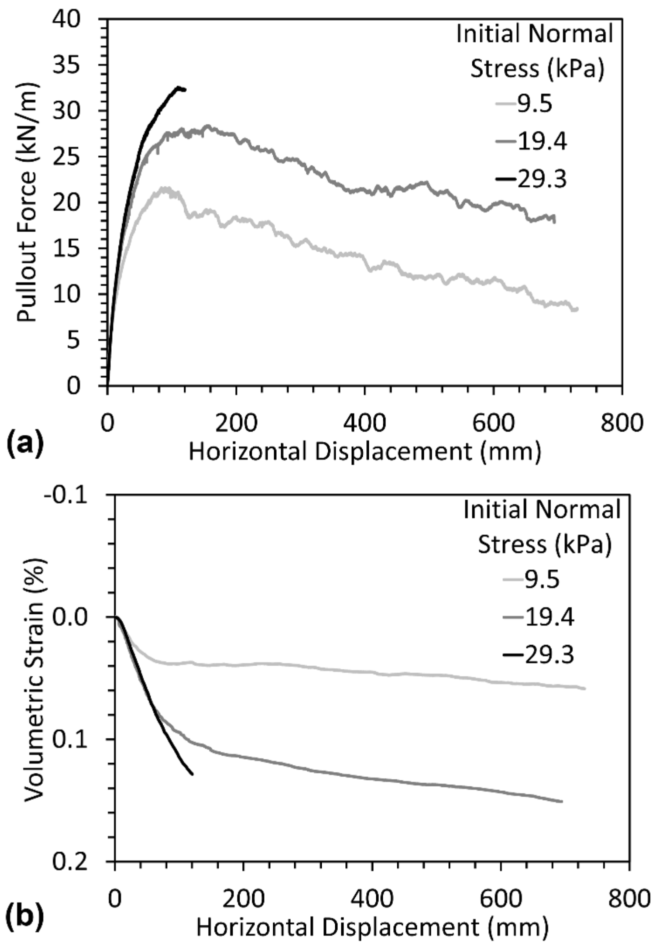

Figure 12: Pullout results for GGC: (a) Pullout force-displacement curves; (b) Volumetric strain-displacement curves

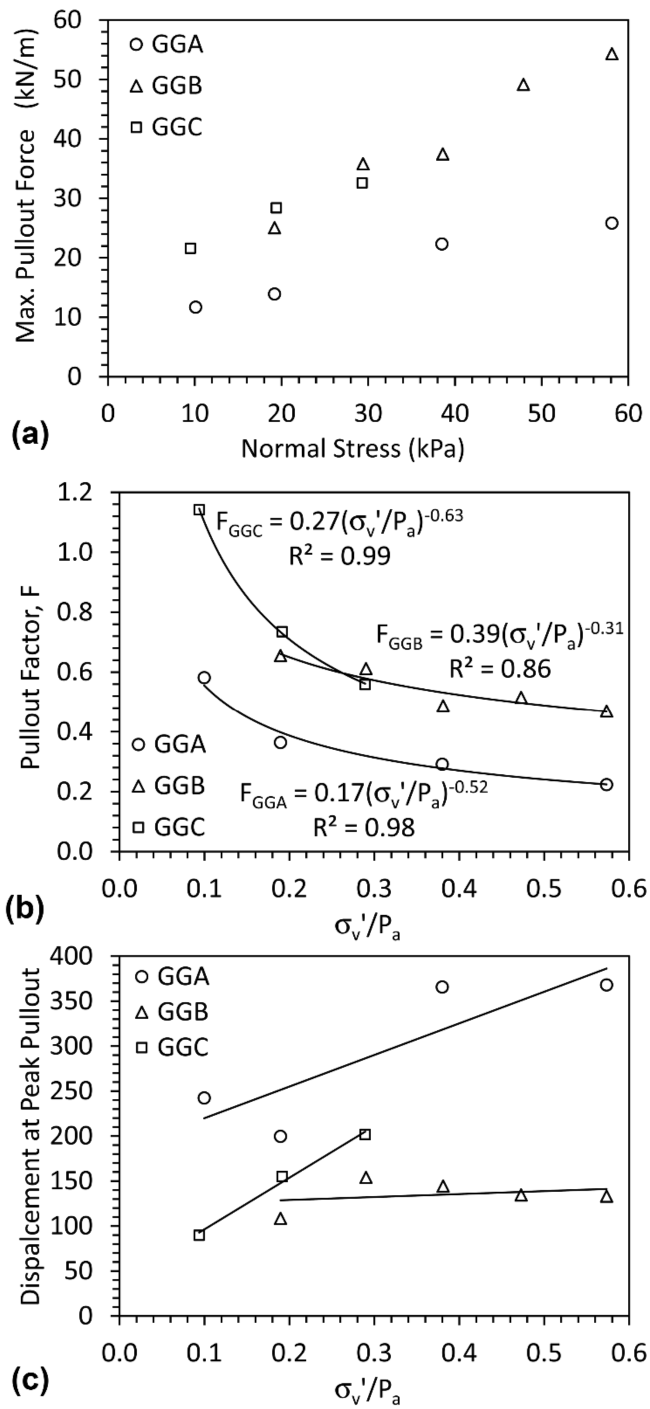

Figure 13: Pullout test synthesis: (a) Maximum pullout force versus normal stress; (b) Pullout factor versus normalized normal stress; (c) Displacement at peak pullout force